This article has been accepted for publication in a future issue of this journal, but has not been fully edited. Content may change prior to final publication. Citation information: DOI 10.1109/TII.2019.2923567, IEEE Transactions on Industrial Informatics

Delta-Bar-Delta Neural Network (NN) Based Control Approach for Power Quality Improvement of Solar PV Interfaced Distribution System

Pavitra Shukl, *Member, IEEE* and Bhim Singh, *Fellow, IEEE*

***Abstract*— A serious concern regarding deterioration in power quality, has emerged with the increasing integration of solar photovoltaic (PV) energy sources to the utility primarily in the scenario of weak distribution grid. Therefore, power quality improvement of the grid tied solar energy conversion system is paramount by implementation of a robust control technique. This work deals with a delta-bar-delta neural network (NN) control for operating optimally by feeding active power to the loads and remaining power to the grid as a function of distribution static compensator (DSTATCOM) capabilities such as mitigating harmonics, balancing of load and improving power factor. The control algorithm provides the ability to adjust weights adaptively in an independent manner and hence it offers alleviation in model complexity predominant during abnormal grid conditions along with reduction in computational time. Moreover, the neural network based control technique offers enhanced accuracy due to the combinational neural structure in the estimation process. In addition, the system performance according to the IEEE-519 standard, has been verified hence, it is proficient in maintaining the power quality. The solar PV array efficient utilization is accomplished through an incremental conductance (INC) based maximum power point tracking (MPPT) technique. For validating the behavior of proposed system, its performance is studied using simulation results. Moreover, a prototype is developed for validation and experimental results corroborate reliable operation under non-ideal grid conditions comprising of wide range of load variations, voltage sag and varying solar insolation conditions.**

***Index Terms*— Solar Photovoltaic (PV) Generation, Power Quality, Delta-Bar-Delta, Neural Network, Distribution Static Compensator (DSTATCOM)**

I. Introduction

The energy has emerged as the backbone of the economic and technological development of the world during the past few years. In accordance with the reports, the population of the world is estimated to grow by 1% in the coming years. However, the gross domestic product (GDP) rise is estimated to be around 3%. Moreover, considering GDP per capita as the global energy demand indicator, the escalating requirement of energy sources, is prevalent [1]. Therefore, with an increase in the energy requirement of the world and the exhaust of fossil fuels (like coal, natural gas and petroleum), the emphasis on renewable energy sources is predominant [2]. In addition, the increasing pollution levels due to an increase in the carbon footprint, is one of the main factors for the inclination towards utilization of renewable energy sources. In order to build a large energy base, there is a need to fully exploit the available renewable energy resources. Currently, the contribution by the renewable energy sources, is around 18% of the world energy demand. However, according to an estimate by the International Energy Agency (IEA), the overall energy requirement of the world, is expected to increase by 50% in the near future [3]. With the reduction in pollution and an increase in grid parity as the major benefits, solar energy is gaining popularity due to the encouragement given by the government, with an increase in government subsidies for their easy installation and operation [4].

The contribution of solar power in terms of meeting the global energy demand is increasing rapidly. During recent years, the major factors include a sharp fall in the cost of silicon, which is the primary resource in the solar power production [5] and an upsurge in technical skill thereby leading to a decrease in the overall solar photovoltaic (PV) cost. Villalva *et al.* [6] have presented the modelling of PV array, where a simple, fast and accurate method is given for realizing the solar PV array. On the other hand, the solar PV array characteristics depict the nonlinear behaviour between its voltage and current. As a result, it is necessary to extract maximum power from the solar PV array by utilizing a maximum power point tracking (MPPT) mechanism in order to ensure that the interfaced power converter is capable of self-adjusting its parameters during run time based on the varying current/voltage levels of the PV source. The realization of MPPT controllers [7] can be based on different methods and algorithms. However, the prevalent techniques include perturb and observe (P&O) [8] and incremental conductance (INC) techniques. Due to the reduced oscillations in INC method while determining the maximum power point (MPP), it is preferred here and it is also suitable for commercial purposes.

The utilization of solar photovoltaic systems, can be grouped into single stage or double stage topologies. However, the benefits of single stage topology, include reduction in cost as the required number of component are less, decrease in losses of the system due to absence of a boost converter and reduction in the overall complexity of the system thereby enhancing the utilization of solar PV array, which makes it a preferable choice over double stage topology as presented by Wu *et al.* in [9]. However, the grid cannot be fed directly with power harnessed from the PV array thus, a power converter like voltage source converter (VSC) is essential for the DC-AC conversion process. Therefore, the combination of solar PV array and VSC at the point of intersection (POI) with utility grid, can be used in standalone and grid-connected systems. In standalone systems, the requirement of additional storage systems (batteries), is due to the nonconformity in time regarding the solar PV output and the energy requirement of the connected loads [10]. However,

This article has been accepted for publication in a future issue of this journal, but has not been fully edited. Content may change prior to final publication. Citation information: DOI 10.1109/TII.2019.2923567, IEEE Transactions on Industrial Informatics

the exclusion of battery storage bank is the primary benefit of grid connected solar PV systems, as the grid is utilized for energy storage [11] resulting in the considerable reduction of maintenance cost as well as initial cost. Nowadays, the rooftop PV systems are being encouraged further due to the key factors of reduction in land requirements and a decrease in size of mounting structures.

Several issues are observed in terms of power quality and reliability in regard with the supplied energy to the utility grid [12]. These issues are observed at load side as well as utility side. Nonlinear loads are connected at the load side, which are a major source of harmonics, disturbances and load unbalancing [13]. Moreover, the grid voltage in addition, suffers from power quality problems of under voltage, over voltage and harmonics due to the irregular and nonlinear loads. These power quality issues lead to financial losses, equipment damage and loss of important data. In order to alleviate the power quality problems, VSC is also utilized as a distribution static compensator (DSTATCOM), which performs the function of power factor improvement and harmonics mitigation through an optimal control technique [14]. There are numerous control techniques, which exist in the literature involving phase locked loops (PLLs) namely quadrature PLL (QPLL), enhanced PLL (EPLL) [15], modified EPLL, dual second order generalized integrator (DSOGI-PLL), fixed frequency PLL (FFPLL) and synchronous reference frame (SRF-PLL) [16]. However, the major drawbacks of PLL techniques, include enhanced complexity, presence of abc to dq transformation, which worsens the dynamic behavior and increases the computational burden. Moreover, this transformation further leads to a sluggish response. The comparative performance of the control mechanism based on Kalman filter is shown in [17]. The control technique based on least mean fourth (LMF) estimation, is shown in [18], where complexity is augmented due to the presence of fourth order optimization technique, which degrades the steady state response. Furthermore, second order generalized integrator (SOGI) based control is presented in [19], which has reduced DC offset reduction capabilities.

The control techniques based on neural network (NN) are gaining importance in recent times. The reduced computational burden and algorithm complexity have been achieved due to the recent advancement in NN. The NN based control algorithms are being utilized for several applications including electrical machines, aircraft landing control due to the accuracy provided by these techniques with the combinational neural structure in the estimation process [20]. Moreover, NN based control techniques are becoming highly popular in grid integration system, in order to make control fast and to increase the decision taking ability. As shown in [21], a synchronous reference frame (SRF) based NN control is presented. For control purpose in the distribution network, the NN structure based on least mean square (LMS) has been proposed by Agarwal *et al.* [22]. The control method based on back propagation (BP) technique is also presented in [23]. However in case of the BP method, all weights are applied with the similar learning rate. Hence, the same change rate is observed for all weights. The Adam optimization based technique is becoming popular however, the increase in complexity and reduction in generalization ability as observed in [24], has limited their usage in the distribution system. Similarly, various integration methods of NN with the conventional control technique are available in the literature. However, the crucial issues existing with these techniques are that the performance under abnormal conditions of grid is not examined which are although, in distributed power generation system a critical phenomenon and are frequent in their occurrence.

In view of that, the delta-bar-delta based neural network (NN) control method is used here, as it is capable of handling nonlinearities, uncertainties, mitigating harmonics and providing satisfactory response during power quality issues [25] arising due to abnormal grid conditions like load unbalancing, voltage sag and variable solar insolation. Moreover, the application of the delta-bar-delta control technique has never been implemented and executed for the aspects of harmonics mitigation and extraction of the active component of load currents. It is also extremely fast in nature as here the weights are updated independently with self-adapting capability. This property is advantageous as in practical situations, where certain weights might be close to optimum and thus they may have a stronger influence on the error gradients. Consequently, a higher speed of convergence and higher flexibility are achieved if these weights are adjustable adaptively in an independent manner. Thus, fast convergence rate and adaptive nature have led to a reduction in computational burden and ease in application. A major advantage also includes improvement in the performance with soft computing NN based control structure without considerable changes required in the hardware, which makes it a desirable choice for commercial purposes by being compact, energy efficient and reliable.

A. Contributions

The key contributions of this work, are summarized as follows with respect to implementation of the delta-bar-delta NN control algorithm.

- For the efficient performance of grid interfaced solar PV system, a delta-bar-delta control algorithm is developed where, the improved proficiency of the control technique is due to the fast extraction of the load active power fundamental component.
- The operation of proposed control method, is observed to be consistent, flexible and robust even during conditions of weak grid. Furthermore, the experimental validation of the developed technique has been performed under various conditions, such as under voltage, variable load conditions and intermittent solar insolation conditions.
- A PV feed-forward term is also included to improve the dynamic response in situations of disturbed atmospheric conditions and the satisfactory performance of the proposed system is validated in accordance to the IEEE 519 standard.

The simulation and training of control technique are executed in MATLAB/Simulink environment utilizing Simscape toolbox based on delta-bar-delta NN method for grid interfaced solar PV system. In order to validate the performance of proposed

This article has been accepted for publication in a future issue of this journal, but has not been fully edited. Content may change prior to final publication. Citation information: DOI 10.1109/TII.2019.2923567, IEEE Transactions on Industrial Informatics

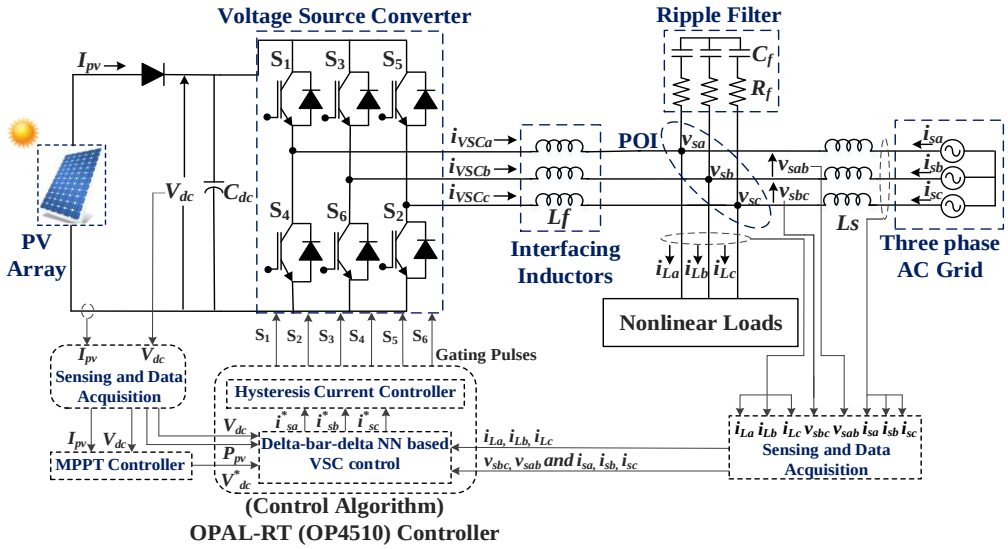

Fig. 1 Proposed system configuration.

system under weak grid conditions, a laboratory prototype is developed and satisfactory results are obtained in accordance to the IEEE 519 standard [26] for conditions like varying solar insolation conditions, load unbalancing and voltage sag.

II. System Configuration

The system configuration is represented in Fig. 1. It consists of a solar PV (PV) array, which is utilized under standard test conditions. Moreover, in order to utilize the solar PV array at maximum power, a maximum power point tracking technique (MPPT) is used based on incremental conductance (INC) method. A VSC is used for interfacing the single stage solar PV energy conversion system with three phase utility grid connected and nonlinear loads at the point of intersection (POI). It is interfaced through an inductor (L_f) in order to mitigate the current harmonics present in the proposed system. In addition, a ripple filter consisting of R_f, C_f is linked in shunt at the POI for alleviating the switching ripples. The VSC consists of insulated gate bipolar transistors (IGBTs) based switches (S_1-S_6), where the switching pulses are governed by the generated reference currents (i^*_{sa}, i^*_{sb}, i^*_{sc}) with the proper application of delta-bar-delta NN based control. With the help of the delta-bar-delta control, an efficient extraction of the load current active power component is achieved, which is utilized in estimation of the active power component of the grid currents. Subsequently, it is used for the generation of switching pulses of VSC. Hence, in order to enhance the VSC efficiency, it is imperative to utilize an adaptive control algorithm. The experimental and simulation parameters utilized for corroboration of the proposed system, are given in Appendix.

III. Control Algorithm

As depicted in Fig. 2, the grid tied solar PV system is implemented using a control structure. The maximum power point is determined through the use of an incremental conductance (INC) method in order to improve the efficiency of the solar PV array. The extraction of fundamental load active power component is achieved through the usage of a delta-bar-delta NN control algorithm as depicted in Fig. 3. The estimation of reference grid currents, is performed by the control approach through appropriate switching of VSC, and therefore, the harmonics are eliminated in the proposed system. The detailed control structure is composed of (a) MPPT controller of a solar PV array utilizing an incremental conductance technique, (b) calculation of load active power current component, (c) implementation of delta-bar-delta learning technique, (d) assessment of grid currents active power components and generating switching pulses of VSC, as described in the following section.

A. MPPT of Solar PV Array utilizing Incremental Conductance (INC) Technique

A maximum power point tracking (MPPT) algorithm at a particular level of insolation based on incremental conductance (INC) method, is realized in the system. The actual operating point is obtained through INC algorithm as it ceases perturbation on achieving the MPPT. An INC technique is utilized due to its good steady state performance, easy implementation and fast dynamic responses as well as convergence rate. The working of INC based MPPT, is governed according to the following equations,

$$\frac{dP_{PV}}{dV_{PV}} = -\frac{I_{PV}}{V_{PV}}, \frac{dP_{PV}}{dV_{PV}} = 0 \text{ therefore, } V_{MPPnew} = V_{MPPold} \quad (1)$$

$$\frac{dP_{PV}}{dV_{PV}} > \frac{-I_{PV}}{V_{PV}}, \frac{dP_{PV}}{dV_{PV}} > 0 \text{ therefore, } V_{MPPnew} = V_{MPPold} + \Delta V_{MPP} \quad (2)$$

$$\frac{dP_{PV}}{dV_{PV}} < \frac{-I_{PV}}{V_{PV}}, \frac{dP_{PV}}{dV_{PV}} < 0 \text{ therefore, } V_{MPPnew} = V_{MPPold} - \Delta V_{MPP} \quad (3)$$

where, the new and old reference DC-link voltages are denoted as V_{MPPnew}, $V_{MPPpold}$ and the past sample values are utilized for subsequent iterations, which are stored as V_{pv} and I_{pv}.

B. Calculation of Active Component of Load Current

The current components of load active power (φ_{as}, φ_{bs}, φ_{cs}), are determined with the usage of delta-bar-delta NN technique from the polluted load currents utilizing supervised and feed-forward principle. Here, the input layer is expressed for the

This article has been accepted for publication in a future issue of this journal, but has not been fully edited. Content may change prior to final publication. Citation information: DOI 10.1109/TII.2019.2923567, IEEE Transactions on Industrial Informatics

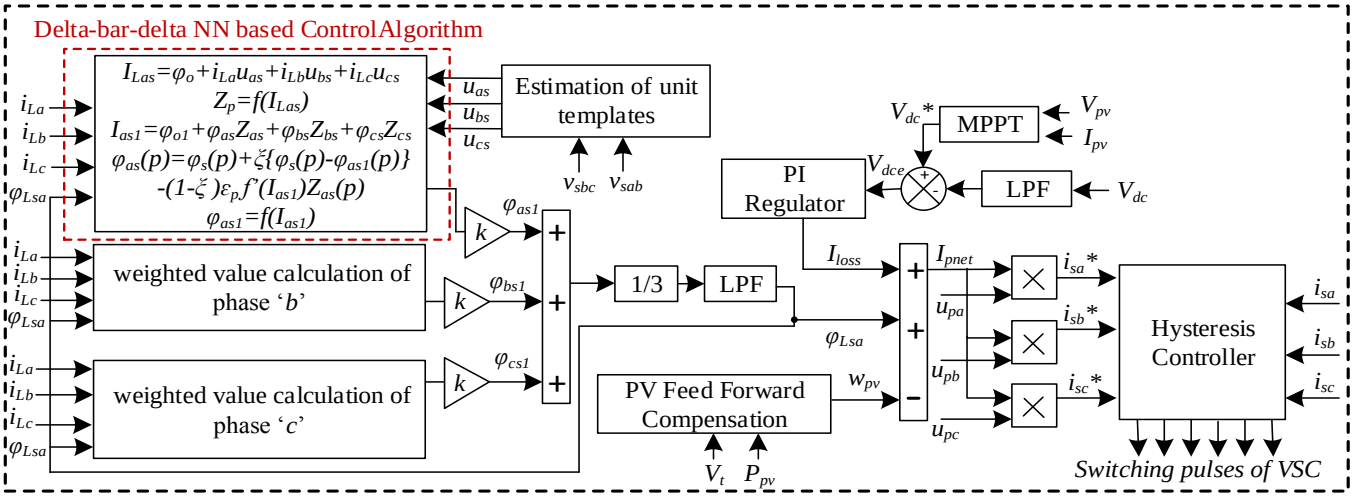

Fig. 2 Block diagram of Delta-Bar-Delta NN based control structure.

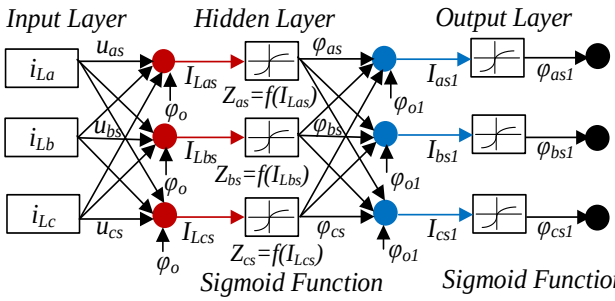

Fig. 3 Proposed model of Delta-Bar-Delta NN based extraction of weighted fundamental load active power components.

three phases as,

$$\begin{bmatrix} I_{Las} \\ I_{Lbs} \\ I_{Lcs} \end{bmatrix} = \begin{bmatrix} \varphi_o \\ \varphi_o \\ \varphi_o \end{bmatrix} + \begin{bmatrix} u_{as} & u_{bs} & u_{cs} \\ u_{bs} & u_{cs} & u_{as} \\ u_{cs} & u_{as} & u_{bs} \end{bmatrix} \begin{bmatrix} i_{La} & i_{Lb} & i_{Lc} \\ i_{Lb} & i_{Lc} & i_{La} \\ i_{Lc} & i_{La} & i_{Lb} \end{bmatrix} \quad (4)$$

Accordingly, here φ_o is the bias weight and u_{as}, u_{bs}, u_{cs} are the unit templates in-phase with the POI phase voltages.

Therefore, for estimating in-phase templates, the line voltages (v_{sab}, v_{sbc}) are sensed and utilized. For determination of phase voltages (v_{sa}, v_{sb}, v_{sc}), these line voltages (v_{sab}, v_{sbc}) are used as,

$$v_{sa}=(2v_{sab}+v_{sbc})/3, v_{sb}=(-v_{sab}+v_{sbc})/3, v_{sc}=(-v_{sab}-2v_{sbc})/3 \quad (5)$$

Hence, the amplitude of terminal voltage (V_t) is determined as,

$$\text{where, } V_t=\sqrt{2(v_{sa}^2+v_{sb}^2+v_{sc}^2)/3} \quad (6)$$

The evaluation of unit templates, is performed using these calculated terminal voltage and grid phase voltages, which are in-phase with POI as,

$$u_{as}=v_{sa}/V_t, u_{bs}=v_{sb}/V_t, u_{cs}=v_{sc}/V_t \quad (7)$$

The extracted I_{Las}, I_{Lbs}, I_{Lcs} are further passed through an activation function (sigmoid function) and the output signals are obtained from the feed-forward segment are denoted as Z_{as}, Z_{bs}, Z_{cs}.

$$Z_{as}=f(I_{Las}), Z_{bs}=f(I_{Lbs}), Z_{cs}=f(I_{Lcs}) \quad (8)$$

$f(I_{Las})=1/(1+e^{-I_{Las}})$, $f(I_{Lbs})=1/(1+e^{-I_{Lbs}})$, $f(I_{Lcs})=1/(1+e^{-I_{Lcs}})$ are the output signals of sigmoid function.

The hidden layer is fed with these estimated values of Z_{as}, Z_{bs}, Z_{cs} hence, the signals obtained before providing to the activation function, are given as,

$$\begin{bmatrix} I_{as1} \\ I_{bs1} \\ I_{cs1} \end{bmatrix} = \begin{bmatrix} \varphi_{o1} \\ \varphi_{o1} \\ \varphi_{o1} \end{bmatrix} + \begin{bmatrix} \varphi_{as} & \varphi_{bs} & \varphi_{cs} \\ \varphi_{bs} & \varphi_{cs} & \varphi_{as} \\ \varphi_{cs} & \varphi_{as} & \varphi_{bs} \end{bmatrix} \begin{bmatrix} Z_{as} & Z_{bs} & Z_{cs} \\ Z_{bs} & Z_{cs} & Z_{as} \\ Z_{cs} & Z_{as} & Z_{bs} \end{bmatrix} \quad (9)$$

Here, φ_{o1}, φ_{as}, φ_{bs}, φ_{cs} are the bias weights of hidden layer and the updated weights of three phases, respectively.

C. Implementation of Delta-Bar-Delta Learning Technique

The φ_{as}, φ_{bs}, φ_{cs} are obtained by utilizing the average load current active power weighted value (φ_{Lsa}). At the p^{th} sampling instant, the updated weight of phase 'a' is determined as,

$$\Delta\varphi(p)=\xi\Delta\varphi(p-1)-(1-\xi)\varepsilon_p f'(I_{as1})Z_{as}(p) \quad (10)$$

For p^{th} sampling instant, the resultant derivative d_p determines the current error gradient. The error to be minimized by the momentum based optimization with delta-bar-delta learning technique, is represented as,

$$E_a(p)=i_{La}(p)-u_{as}(p)\varphi_{as1}(p) \quad (11)$$

For the past error derivatives, the exponential average is denoted by f_p which governs in which direction, the error has been decreasing which is expressed as follows.

$$f_p=\theta f_{p-1}+(1-\theta)d_{p-1} \quad (12)$$

For the exponential average of the past derivatives, the weighting is determined by θ and the weighting on the last derivative is controlled by (1-θ). Therefore, the weightings influence whether the distant gradients have a stronger influence or the most recent ones on the f_p. This concept is reflected by the delta-bar-delta learning method, thereby allowing only smaller adjustments, when $d_p f_p$ is negative and allowing larger modifications in the learning rate ε_p, in which $d_p f_p$ is positive as shown in,

$$\varepsilon_p=\begin{cases} \varepsilon_{p-1}+\kappa & \text{for } d_p f_p>0 \\ \varepsilon_{p-1}\times\phi & \text{for } d_p f_p\le 0 \end{cases} \quad (13)$$

Consequently, the new weight change is observed as soon as the new learning rate ε_p is decided and d_p is composed of $f'(I_{as1})Z_{as}(p)$. In order to adjust the weights adaptively, the momentum based optimization approach is applied during delta-bar-delta learning for obtaining the optimum weights.

This article has been accepted for publication in a future issue of this journal, but has not been fully edited. Content may change prior to final publication. Citation information: DOI 10.1109/TII.2019.2923567, IEEE Transactions on Industrial Informatics

During online training of weights, this technique realizes the new weight increment by superimposing the average of the past weight changes and thus, the net weight change is smoothened out. Thus, the updated weight of phase '*a*' is represented as,

$$\varphi_{as}(p)=\varphi_{Lsa}(p)+\xi\{\varphi_{Lsa}(p)-\varphi_{as1}(p)\}-(1-\xi)\varepsilon_p f'(I_{as1})Z_{as}(p) \quad (14)$$

Accordingly, $\varphi_{Lsa}(p)$ and $\varphi_{as}(p)$ are the active power component average weighted value and the phase '*a*' updated weighted value at p^{th} sampling instant, respectively. Moreover, $Z_{as}(p)$ and $\varphi_{as1}(p)$ are the output of feed-forward section and the weighted amplitude of the load current active power, respectively. The momentum is denoted as ξ, learning rate is represented by ε_p and $f'(I_{as1})$ is the derivative of I_{as1} component. Moreover, the values of κ as 0.1, ϕ as 0.5 and θ as 0.7 are taken, as for wide range of problems these set of values work well.

Therefore during optimization, the momentum term ξ indicates the relative importance of the past weight change on the new weight increment. Thus, the new weight increment is decided by the current gradient and the past weight change together. For instance, the momentum does not apply at all and the past history has no place if ξ is equal to 0. However, the current change is totally based on the past change, if ξ is equal to 1. Moreover, the combined response to weight change is obtained if the values of ξ lie between 0 and 1. Consequently, each previous weight change would depend on the change prior to that and all the way back to the first change hence, exhibiting that all the weight changes are recursive. The oscillations are minimized in the obtained error as the momentum accelerates the current weight change, which thus improves the accuracy. The need for adjusting weights adaptively can be accounted for providing a quick response in case of abnormal utility grid conditions and hence, ensuring satisfactory performance of the proposed system.

Correspondingly, the updated weights for remaining phases are expressed as,

$$\varphi_{bs}(p)=\varphi_{Lsa}(p)+\xi\{\varphi_{Lsa}(p)-\varphi_{bs1}(p-1)\}-(1-\xi)\varepsilon_p f'(I_{bs1})Z_{bs}(p) \quad (15)$$

$$\varphi_{cs}(p)=\varphi_{Lsa}(p)+\xi\{\varphi_{Lsa}(p)-\varphi_{cs1}(p-1)\}-(1-\xi)\varepsilon_p f'(I_{cs1})Z_{cs}(p) \quad (16)$$

The I_{as1}, I_{bs1}, I_{cs1} are the extracted values, which are then supplied to the sigmoid function for the estimation of active fundamental component,

$$\varphi_{as1}=f(I_{as1})=1/(1+e^{-I_{as1}}) \quad (17)$$

$$\varphi_{bs1}=f(I_{bs1})=1/(1+e^{-I_{bs1}}) \quad (18)$$

$$\varphi_{cs1}=f(I_{cs1})=1/(1+e^{-I_{cs1}}) \quad (19)$$

A scaling factor of '*k*' is used as presented in Fig. 3, in order to obtain the actual value (φ_{as1}) since the output obtained from the activation function is in the range of 0 to 1.The amplitude of average active power fundamental component (φ_{Lsa}) is calculated by utilizing φ_{as1}, φ_{bs1}, φ_{cs1}.

$$\varphi_{Lsa}=(\varphi_{as1}+\varphi_{bs1}+\varphi_{cs1})/3 \quad (20)$$

In order to separate low-frequency components, a low pass filter of first order is utilized. The calculated output is termed as average amplitude of weighted active power component and it is denoted as φ_{Lsa}.

D. Assessment of Grid Currents Active Power Components and Switching Pulses Generation of VSC

The DC link voltage error is evaluated by subtracting the reference voltage (V^*_{dc}) and the sensed voltage (V_{dc}) as,

$$V_{dce}=V^*_{dc}(m)-V_{dc}(m) \quad (21)$$

Here, maximum power point tracking (MPPT) of the solar PV array is utilized for obtaining the reference voltage level (V^*_{dc}). The voltage of DC link, is sensed by voltage sensor and is represented as V_{dc}. Moreover, by feeding V_{dce} to the proportional-integral (PI) controller, the voltage error (V_{dce}) is utilized for estimating DC loss component,

$$I_{loss}(m)=I_{loss}(m-1)+K_p\{V_{dce}(m)\}+K_i\{V_{dce}(m)-V_{dce}(m-1)\} \quad (22)$$

Here, PI controller gains are designated as K_i (integral gain) and K_p (proportional gain).

The dynamic behaviour of PV system is improved by incorporating a PV power feed-forward term (w_{pv}) as,

$$w_{pv}=(2P_{pv})/(3V_t) \quad (23)$$

where, V_t, P_{pv} denote the terminal voltage and power obtained from a PV array, respectively. The grid active power component is calculated using average active power load current component (φ_{Lsa}), PV feed-forward term (w_{pv}) and loss component (I_{loss}),

$$I_{pnet}=\varphi_{Lsa}+I_{loss}-w_{pv} \quad (24)$$

The reference grid currents are estimated utilizing grid active power component and in-phase unit templates as,

$$i^*_{sa}=I_{pnet}\times u_{as}, i^*_{sb}=I_{pnet}\times u_{bs}, i^*_{sc}=I_{pnet}\times u_{cs} \quad (25)$$

Hence, the obtained reference grid currents are subtracted from the actual grid currents for error estimation,

$$i_{esa}=i^*_{sa}-i_{sa}, i_{esb}=i^*_{sb}-i_{sb}, i_{esc}=i^*_{sc}-i_{sc} \quad (26)$$

For switching of VSC, the hysteresis current controller generates the switching pulses by utilizing these errors.

E. Comparative Performance of Proposed Control with Existing Control Algorithms

Fig. 4 illustrates the comparative performance with existing control algorithms. The system operation is presented for both dynamic and steady-state conditions. The load active component (φ_{as1}) is shown during load unbalancing condition. Hence, load unbalance in phase '*a*' is considered from 0.5s to 1s, which shows the performance during dynamic condition. Therefore, it can be seen from these results that proposed delta-bar-delta control algorithm provides fast, smooth and oscillation free active power component of load current. As when the load in phase '*a*' is removed then oscillations are observed in SRFT control and erroneous estimation with oscillations, is observed in LMS based NN control. Similarly, during load injection conditions due to faster convergence, the performance of delta-bar-delta is observed better as compared to other algorithms. Thus, both dynamic and steady-state performances of the system, are improved as oscillations with delta-bar-delta NN control are damped efficiently. Table I depicts the comparative performance of the control schemes.

This article has been accepted for publication in a future issue of this journal, but has not been fully edited. Content may change prior to final publication. Citation information: DOI 10.1109/TII.2019.2923567, IEEE Transactions on Industrial Informatics

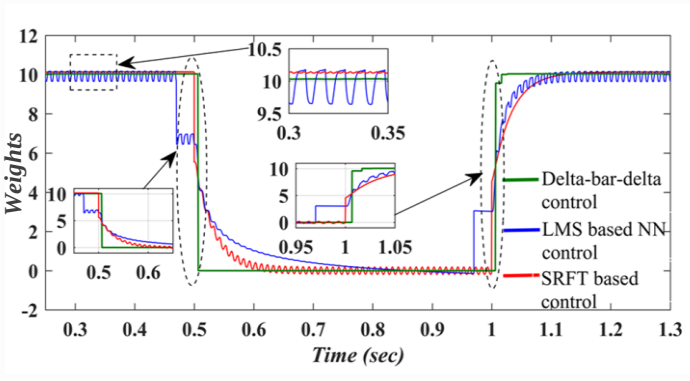

Fig. 4 Comparative Performance of proposed Delta-Bar-Delta control with other existing control algorithms.

TABLE I. COMPARISON OF PARAMETERS OF PROPOSED DELTA-BAR-DELTA CONTROL WITH CONVENTIONAL CONTROL ALGORITHMS

Parameters	**Proposed delta-bar-delta control**	**LMS Technique**	**SRFT control method**
Response under unbalanced load	undistorted	distorted	distorted
Dynamic response	fast	fast	slow
Requirement of PLL	No	No	Yes
Weight convergence	Fast	Fast	Slow
Grid current THD	low	high	medium
Oscillations	low	medium	high
Computational burden	medium	less	high

IV. SIMULATION RESULTS

The modelling and simulation of grid interfaced solar PV system are done using MATLAB/Simulink. The waveforms of grid currents (i_{sabc}), three phase grid voltages (v_{sabc}), VSC currents (i_{VSCabc}), load currents (i_{Labc}), DC link voltage (V_{dc}), solar array power (P_{pv}), solar array current (i_{pv}), solar insolation (G), loss component (I_{Loss}), solar PV feed forward term (w_{pv}) are analysed for validating the satisfactory performance of the proposed system. For validation of the proposed system, the performance is verified in cases of variable solar insolation and unbalanced loading conditions. In Fig. 2, the mechanism for VSC switching pulses, is represented. The estimation of active power component of the load current, is the main function of delta-bar-delta NN control technique. Here, nonlinear loads are modelled to validate the system operation in the unity power factor (UPF) mode for dynamic conditions. The calculated parameters, which are utilized for the satisfactory performance, are presented in Appendix.

A. Behavior at Unbalanced Nonlinear Load

By opening one of the load lines (phase '*a*'), the load disturbance condition is emulated, which emulates unbalanced load and causes reduction in the effective load. In Figs. 5 (a-c), the phase '*a*' load is disconnected at 0.5s in case of nonlinear load unbalanced condition. Therefore, as shown in Fig. 5 (a), the load current of phase '*a*' is equal to zero. After load removal condition, an increase in the grid currents (i_{sabc}) is observed as the net power being fed to the grid increases. However, the grid currents are maintained sinusoidal in case of load unbalancing. Moreover, in '*a*' phase VSC current (i_{VSCa}), a change in the wave-shape can be observed, where it becomes sinusoidal as VSC need not feed any harmonics current in phase *'a'* after load removal. The DC link voltage is maintained constant during this unbalance, with the use of output of PI controller as shown in Fig. 5 (b). No change is observed in PV power, PV current and solar insolation due to unbalanced load condition. In Fig. 5 (c), the waveform of the extracted active power component of load current (φ_{as1}) is depicted and the dynamics in u_{as} remains unchanged. However, the loss component (I_{Loss}) shows a slight change during the unbalanced load condition. The reference grid currents obtained are sinusoidal in nature and for '*a*' phase an increase in the grid and reference currents, is observed, due to a decrease in the load currents.

B. Behavior at Variable Solar Insolation and Nonlinear Load

The nonlinear loads are connected at POI, as presented in Figs. 6 (a-c), under variable solar insolation. At 1.3s, the change in solar insolation level is observed from 1000 W/m^2 to 800 W/m^2. A decrease in solar array current can be observed, therefore, the solar array power is reduced while the load power consumption remains same and hence, the grid currents (i_{sabc}) are decreased in Fig. 6 (a). As shown in (Fig. 6 (b)), decreasing solar insolation, leads to a subsequent reduction in VSC currents (i_{VSCa}, i_{VSCb}, i_{VSCc}). In accordance with the reference value obtained from the MPPT, the DC link voltage is maintained constant. With a decrease in solar insolation, the solar PV power (P_{pv}), solar PV current (I_{pv}) are decreased. As shown in Fig. 6 (c), the internal control signals are observed where the load current active power components do not experience any change during changing solar insolation condition. The in-phase unit template (u_{as}) is maintained sinusoidal. A slight change is observed in the loss component (I_{loss}). Moreover, the reference grid current of '*a*' phase (i_{sa}^*) is observed to decrease in magnitude during the decrease in solar insolation. Similarly, the reference currents of remaining phases are decreased due to the decreasing solar insolation condition. The decrease in the grid current of phase '*a*', has also been shown.

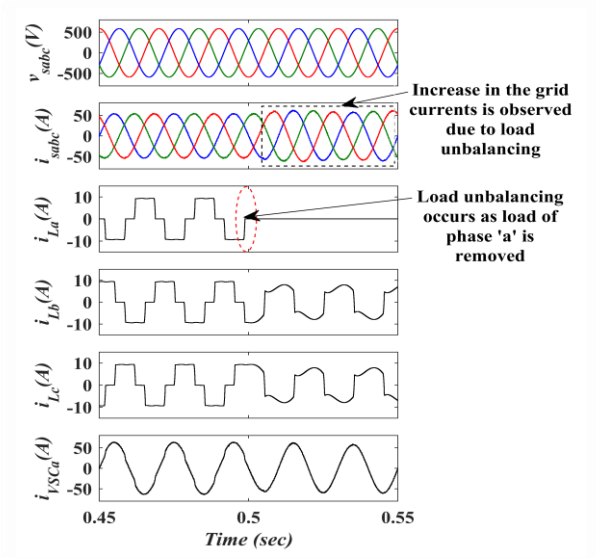

(a)

This article has been accepted for publication in a future issue of this journal, but has not been fully edited. Content may change prior to final publication. Citation information: DOI 10.1109/TII.2019.2923567, IEEE Transactions on Industrial Informatics

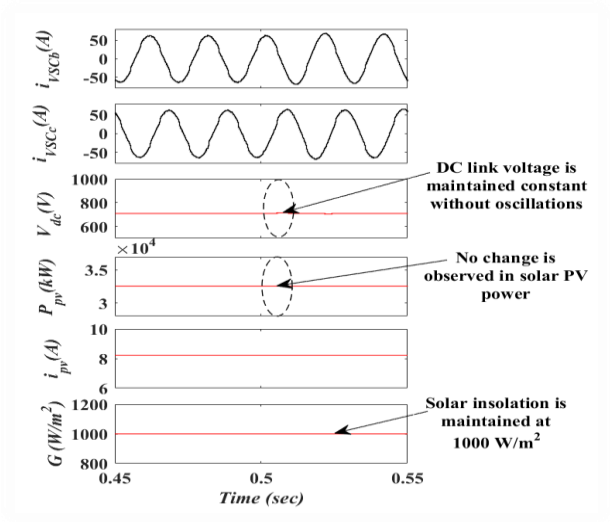

(b)

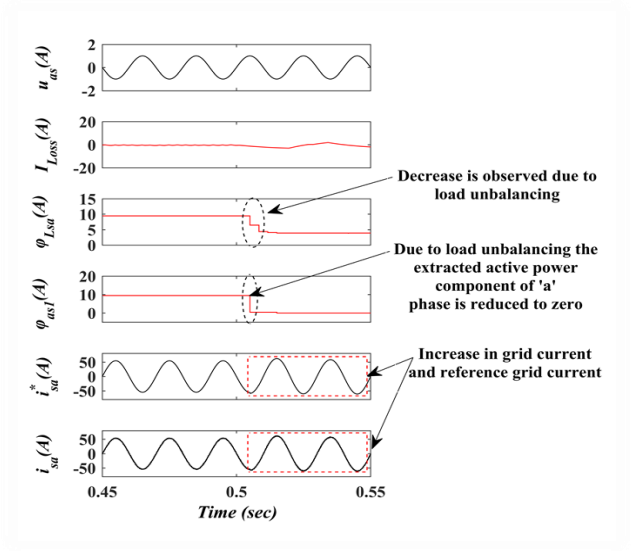

(c)

Fig. 5 Response under unbalanced nonlinear load of grid connected solar PV system.

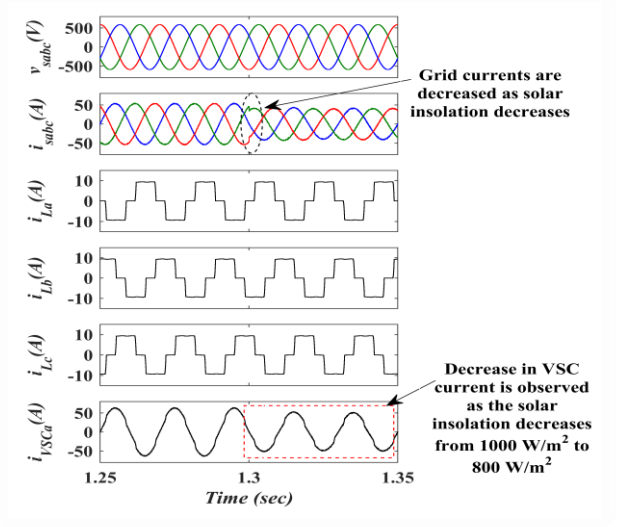

(a)

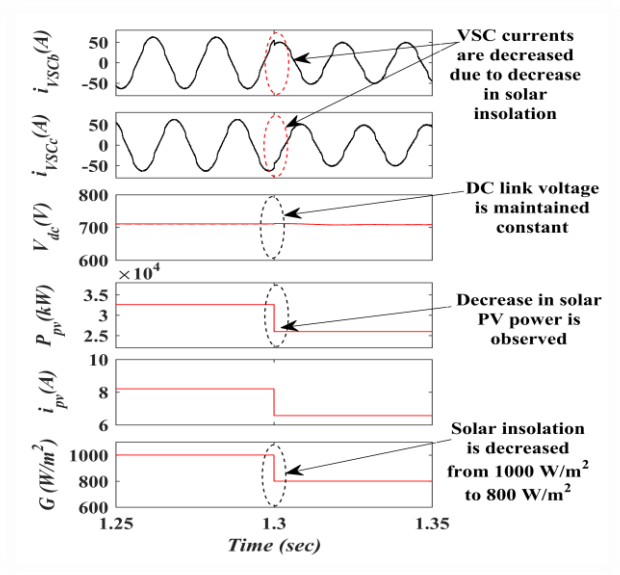

(b)

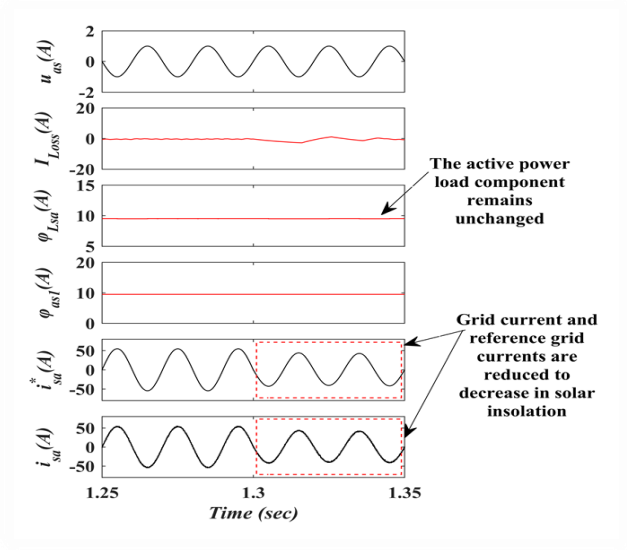

(c)

Fig. 6 Response under variable solar condition of grid connected solar PV system at nonlinear load.

V. Experimental Results

The components of the hardware prototype, include a solar PV array simulator, voltage source converter (VSC), ripple filters, three phase AC grid and nonlinear load. With the use of Hall Effect sensors (LA55-P, LV25-P), the current and voltage of the system, are sensed, respectively. The OPAL-RT controller (OP4510), is used with these sensed signals through analog to digital converters (ADCs), where the signals are processed according to the control algorithm loaded on field programmable gate array (FPGA). Hence, the generated switching pulses of VSC, are supplied through digital inputs and outputs (DIO) to optocouplers. The optocouplers provide isolation between power circuit in the system and OPAL-RT. The IGBTs in VSC, are operated in accordance with the switching pulses generated in the system. The PQ analyser and digital signal oscilloscope (DSO), are utilized for recording the

This article has been accepted for publication in a future issue of this journal, but has not been fully edited. Content may change prior to final publication. Citation information: DOI 10.1109/TII.2019.2923567, IEEE Transactions on Industrial Informatics

performance of the proposed system. For the solar insolation of 1000 W/m^2, in Fig. 7, the behavior of MPPT is presented. As specified in Appendix, the calculated parameters are presented.

A. Operation of System at Steady-State

Figs. 8 (a-i) show the operation under steady-state of the proposed system at nonlinear load. As shown in Fig. 8 (a), the grid current of 4.92A flows into the grid. The grid current total harmonic distortion (THD) is less than 5 %, which is observed to be within the limits of the IEEE-519 standard. As the power is being absorbed by the grid, the grid power is observed with negative sign (Fig. 8 (b)). Fig. 8 (c) shows VSC current as 8.2A and VSC power is observed as 3.11kW in Fig. 8 (d). The solar PV array is responsible for delivering power to the grid and to the connected loads in the distribution system, which is referred to as VSC power. In Fig. 8 (e) and Fig. 8 (f), the load current and load power are observed, respectively. The THD of grid voltage (v_{sab}) is observed in Fig. 8 (g) and it is observed to be 1.8% when the grid voltage considered is 220V. The grid current THD is observed in Fig. 8 (h) which is equal to 3.4 %. Due to the presence of nonlinear load in the system, THD of load current is 27.3% as seen in Fig. 8 (i).

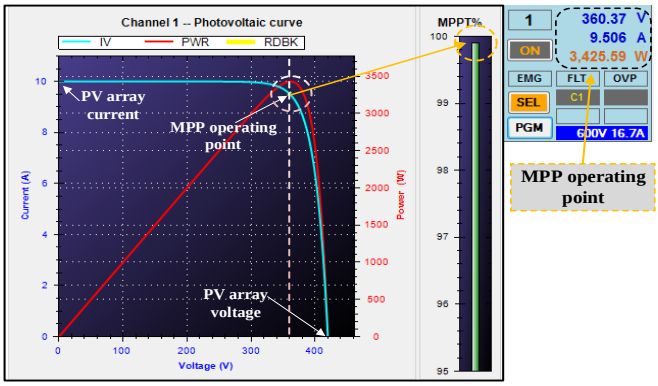

Fig. 7 Performance at solar insolation of 1000 W/m^2 of MPPT.

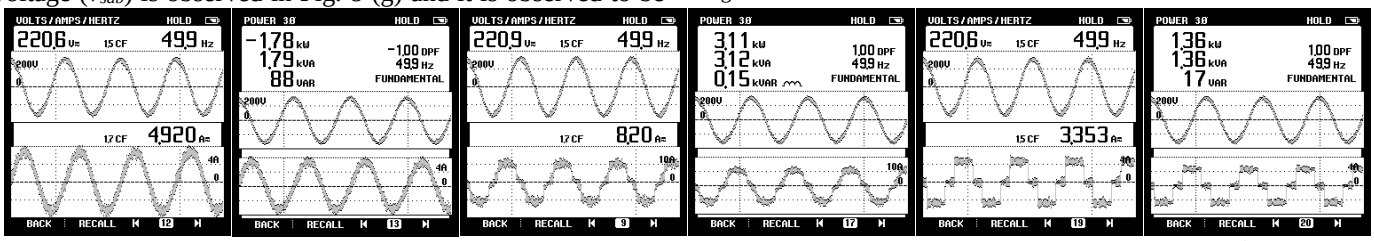

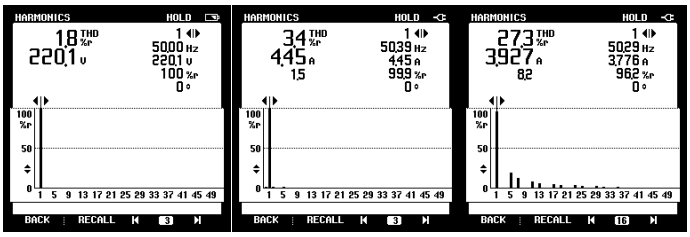

Fig. 8 (a) v_{sab} along with i_{sc} (b) Power of grid (P_g) (c) v_{sab} along with i_{VSCc} for nonlinear loads (d) VSC power (P_{VSC}) (e) v_{sab} along with i_{Lc} (f) Power of load (P_L) (g) For v_{sab}, harmonic spectrum (h) For i_s, harmonic spectrum (i) For i_L, harmonic spectrum.

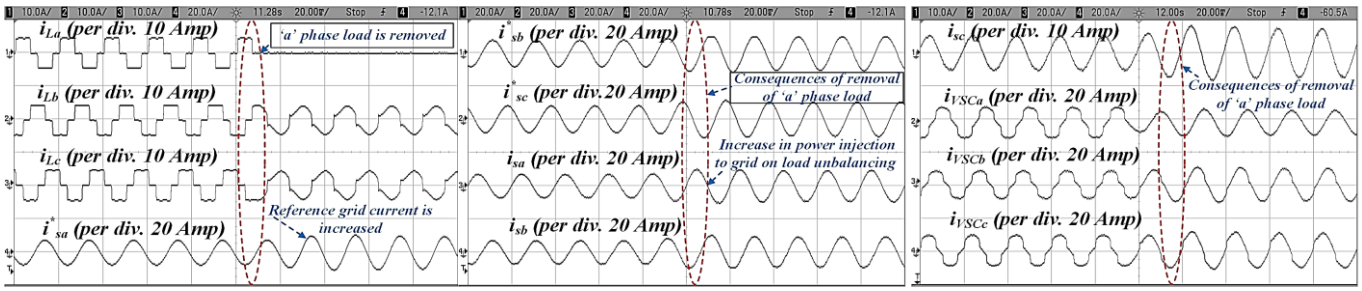

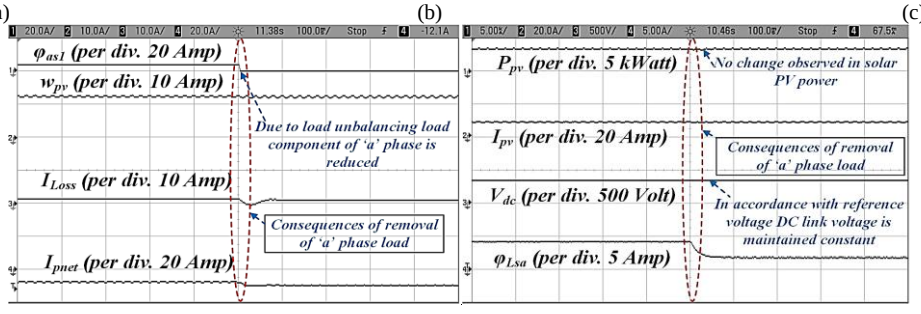

Fig. 9 Behavior of solar PV system from load balanced to load unbalanced condition (a) i_{La}, i_{Lb}, i_{Lc} and i^*_{sa} (b) i^*_{sb}, i^*_{sc}, i_{sa} and i_{sb} (c) i_{sc}, i_{VSCa}, i_{VSCb} and i_{VSCc} (d) φ_{as1}, w_{pv}, I_{Loss} and I_{pnet} (e) P_{pv}, I_{pv}, V_{dc} and φ_L

This article has been accepted for publication in a future issue of this journal, but has not been fully edited. Content may change prior to final publication. Citation information: DOI 10.1109/TII.2019.2923567, IEEE Transactions on Industrial Informatics

B. Dynamic Response of System at Load Removal

The removal of phase '*a*' load is observed by suddenly disconnecting load in Figs. 9 (a-e). The sudden disconnection of the load current is presented by removing phase '*a*' load and the reference grid currents (i^*_{sa}, i^*_{sb}, i^*_{sc}), load currents of remaining phases (i_{Lb}, i_{Lc}) are shown in Figs. 9 (a-b). At the instant of removing load, an increase in grid currents (i_{sa}, i_{sb}, i_{sc}), is observed (Fig. 9 (b)). The dynamics in VSC currents (i_{VSCa}, i_{VSCb}, i_{VSCc}) are shown in Fig. 9 (c), where VSC current of '*a*' phase is observed to be sinusoidal as it does not have to supply harmonic current in phase '*a*'. The control signals during unbalanced load, are shown in Fig. 9 (d), where the load is suddenly removed and, therefore, a decrease in φ_{as1} is observed during this instant. Consequently, φ_{Lsa} is slightly decreased. However, there is no change observed in solar PV current (I_{pv}) and solar power (P_{pv}) as observed in Fig. 9 (e). Moreover, V_{dc} is maintained, in accordance with the reference DC link voltage (Fig. 10 (e)).

C. Behavior of System under Voltage Sag at Nonlinear Load

At voltage sag in Figs. 10 (a-f), the operation of the system under nonlinear load is presented. The performance under a decrease in grid voltage, is shown in Fig. 10 (a). The V_{dc} is maintained at reference voltage under voltage sag condition in Fig. 10 (b). The solar array voltage, solar array power and solar array current have no change during this condition. The system performs satisfactorily under the voltage sag condition as the grid currents are observed sinusoidal in nature. However, an increase in grid currents, is seen in Figs. 10 (c-e). Moreover, the reference currents obtained are sinusoidal in nature and hence the harmonics have been reduced. In Fig. 10 (f), various internal signals depict control algorithm performance under the voltage sag conditions. In Fig. 10 (f), the current loss component is less than 1A and the waveform of extracted load current fundamental active power component φ_{as1} is also presented.

D. Behavior at Variable Solar Insolation and Nonlinear Load

The decrease in solar insolation from 1000 W/m^2 to 800 W/m^2 is presented by waveforms of Figs. 11 (a-e). There is no change observed in grid voltage (v_{sab}), terminal voltage (V_t) due to the changing solar insolation conditions. The reference grid currents are reduced in magnitude as presented in Fig. 11 (b), which are generated by the control approach. In addition, Fig. 11 (b) shows a decrease in magnitude of the grid currents due to the decrease in insolation and a reduction in w_{pv} and I_{pv} is also observed. In Fig. 11 (c), the internal signals are observed with the decrease in solar insolation. As observed in Fig. 11 (d), V_{dc} is maintained almost constant by using a PI controller for satisfactory performance. In Fig. 11 (e), a decrease in VSC (i_{VSCa}, i_{VSCb}, i_{VSCc}) currents, is presented due to decrease in solar irradiation.

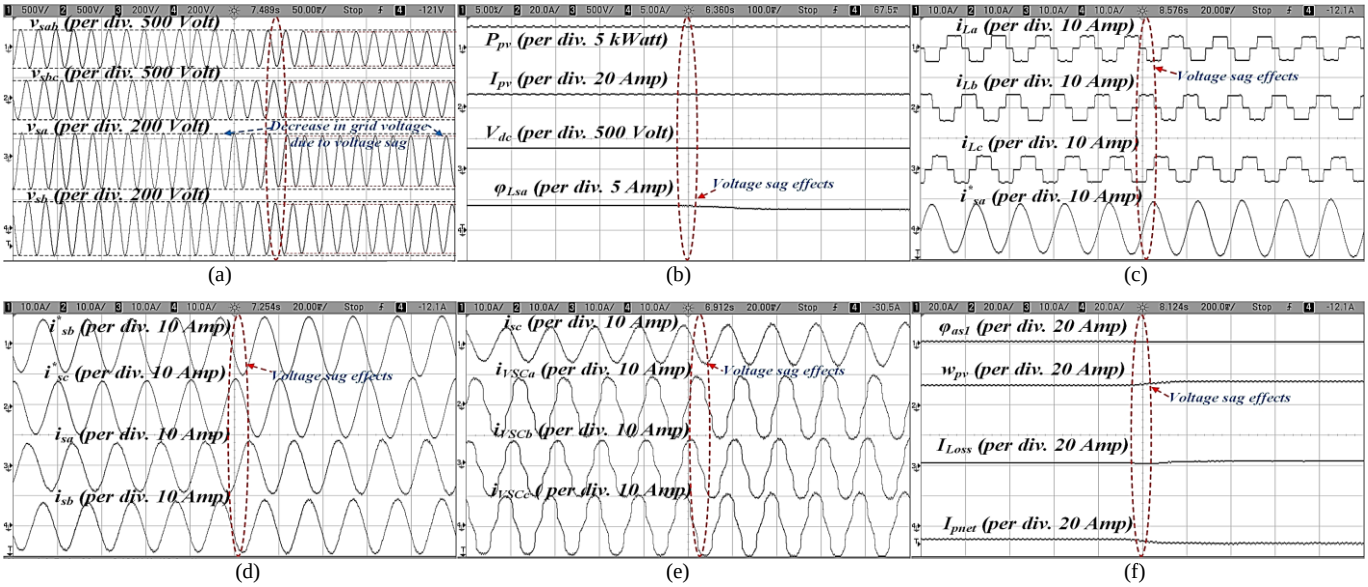

Fig. 10 Behavior of solar PV system under voltage sag (a) v_{sab}, v_{sbc}, v_{sa}, and v_{sb} (b) P_{pv}, I_{pv}, V_{dc} and φ_{Lsa} (c) i_{La}, i_{Lb}, i_{Lc} and i^*_{sa} (d) i^*_{sb}, i^*_{sc}, i_{sa} and i_{sb} (e) i_{sc}, i_{VSCa}, i_{VSCb} and i_{VSCc} (f) φ_{as1}, w_{pv}, I_{Loss} and I_{pnet}.

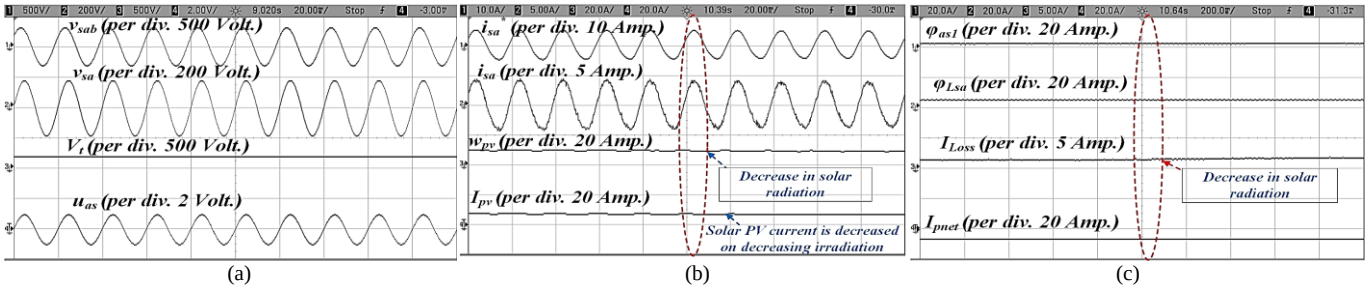

This article has been accepted for publication in a future issue of this journal, but has not been fully edited. Content may change prior to final publication. Citation information: DOI 10.1109/TII.2019.2923567, IEEE Transactions on Industrial Informatics

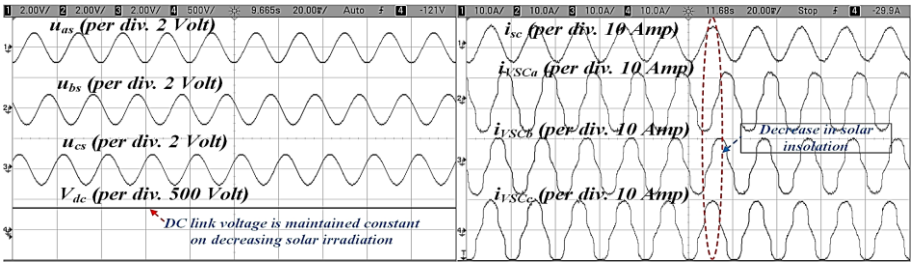

(d) (e)

Fig. 11 For solar irradiation decrease the dynamic behavior of solar PV system (a) v_{sab}, v_{sa} , V_t and u_{as} (b) i_{sa}^*, i_{sa} , w_{pv} and I_{pv} (c) φ_{as1}, φ_{Lsa} , I_{Loss} and I_{pnet} (d) u_{as}, u_{bs}, u_{cs}, *and* V_{dc} (e) i_{sc}, i_{VSCa}, i_{VSCb} and i_{VSCc}.

VI. Conclusion

The delta-bar-delta neural network based control technique has been proposed here for solar PV interfaced to the three phase grid system. The incremental conductance based MPPT has been implemented in order to obtain maximum power from the solar PV array. The control approach performs multiple functions of balancing of load and harmonics elimination. The performance of the grid tied PV system at nonlinear load, has been verified for abnormal conditions of the grid such as under unbalancing of load, decreasing solar insolation and voltage sag conditions. The switching pulses of VSC, are generated by utilizing reference currents obtained by the control structure. The proposed control approach alleviates the complexity of the system and is easy to implement in the system. The grid current THD is obtained in accordance to the IEEE-519 standard and is observed to be less than 5 %. Therefore, for the proposed system, satisfactory performance has been obtained for wide variety of results obtained in steady state and dynamic conditions based on experimental validation.

Appendix

Table II Parameters Of The System

Symbol	Parameter	Value for Simulation	Value for Experiment
V_{sab}	voltage of three-phase grid	415 V	220 V
f_s	frequency of system	50 Hz	50 Hz
R_s	resistance of grid impedance	0.01 Ω	0.01 Ω
L_s	inductance of grid impedance	0.1 mH	0.1 mH
V_{dcref}	reference DC link voltage	700 V	360 V
C_{dc}	capacitance of DC link	6.5 mF	2.21 mF
R_L	resistance of load	70 Ω	120 Ω
L_L	inductance of load	300 mH	160 mH
L_f	interfacing inductance	4 mH	4 mH
R_f	resistance of ripple filter	5 Ω	5 Ω
C_f	capacitance of ripple filter	10 µF	10 µF
K_p	proportional gain	20	2.3
K_I	integral gain	2	0.001
φ_o	bias weight of input layer	0.4	0.4
φ_{o1}	bias weight of hidden layer	0.2	0.2
ξ	momentum	0.6	0.6
P_{pv}	solar PV power	30 kW	3.2 kW
V_{oc}	open circuit voltage	32.9 V	420 V
I_{sc}	short circuit current	8.21 A	10 A
V_{mp}	MPP voltage	26.3 V	360 V
I_{mp}	MPP current	7.61 A	9.48 A
T_s	processing time	10e-6	20e-6

References

[1] Y. Zhang, Y. Wu, D. H. K. Tsang and A. Leon-Garcia, "Guest Editorial Special Section on Energy Informatics for Green Cities," *IEEE Trans. Ind. Informat.*, vol. 14, no. 4, pp. 1456-1457, April 2018.

[2] M. H. Rehmani, M. Reisslein, A. Rachedi, M. Erol-Kantarci and M. Radenkovic, "Integrating Renewable Energy Resources Into the Smart Grid: Recent Developments in Information and Communication Technologies," *IEEE Trans. Ind. Informat.*, vol. 14, no. 7, pp. 2814-2825, July 2018.

[3] A. S. Khan and S. A. Chowdhury, "GHG emission reduction and global warming adaptation initiatives by UNFCCC," *Proc. Int. Conf. Dev. Renew. Ener. Techn.*, pp. 1-6, 2012.

[4] D. Xu, B. Zhou, K. W. Chan, C. Li, Q. Wu, B. Chen and S. Xia, "Distributed Multi-Energy Coordination of Multi-Microgrids with Biogas-Solar-Wind Renewables," *IEEE Trans. Ind.* Informat. Early Access, 2018.

[5] T. K. Chau, S. S. Yu, T. Fernando and H. H. Iu, "Demand-Side Regulation Provision From Industrial Loads Integrated With Solar PV Panels and Energy Storage System for Ancillary Services," *IEEE Trans. Ind. Informat.*, vol. 14, no. 11, pp. 5038-5049, Nov. 2018.

[6] M. G. Villalva, J. R. Gazoli, and E. R. Filho, "Comprehensive approach to modelling and simulation of photovoltaic arrays," *IEEE Trans. Power Electron.*, vol. 24, no. 5, pp. 1198–1208, May 2009.

[7] T. K. Soon and S. Mekhilef, "A Fast-Converging MPPT Technique for Photovoltaic System under Fast-Varying Solar Irradiation and Load Resistance," *IEEE Trans. Ind. Informat.*, vol. 11, no. 1, pp. 176-186, Feb. 2015.

[8] K. Sundareswaran, V. Vigneshkumar, P. Sankar, S. P. Simon, P. Srinivasa Rao Nayak and S. Palani, "Development of an Improved P&O Algorithm Assisted Through a Colony of Foraging Ants for MPPT in PV System," *IEEE Trans. Ind. Informat.*, vol. 12, no. 1, pp. 187-200, Feb. 2016.

[9] T. Wu, C. Chang, L. Lin and C. Kuo, "Power Loss Comparison of Single- and Two-Stage Grid-Connected Photovoltaic Systems," *IEEE Trans. Energy Conv.*, vol. 26, no. 2, pp. 707-715, June 2011.

[10] C. Keerthisinghe, A. C. Chapman and G. Verbič, "Energy Management of PV-Storage Systems: Policy Approximations Using Machine Learning," *IEEE Trans. Ind. Informat.*, vol. 15, no. 1, pp. 257-265, Jan. 2019.

[11] V. N. Lal and S. N. Singh, "Control and Performance Analysis of a Single-Stage Utility-Scale Grid-Connected PV System," *IEEE Sys. Jour.*, vol. 11, no. 3, pp. 1601-1611, Sept. 2017.

[12] K. V. Suslov, N. N. Solonina and A. S. Smirnov, "Distributed power quality monitoring," *Int. Conf. Harmonics Qual. of Power (ICHQP)*, pp. 517-520, 2014.

[13] A. F. Zobaa and S. H. E. Abdel Aleem, "A New Approach for Harmonic Distortion Minimization in Power Systems Supplying Nonlinear Loads," *IEEE Trans. Indus. Inform.*, vol. 10, no. 2, pp. 1401-1412, May 2014.

[14] B. Singh, M. Kandpal and I. Hussain, "Control of Grid Tied Smart PV-DSTATCOM System Using an Adaptive Technique," *IEEE Trans. Smart Grid*, vol. 9, no. 5, pp. 3986-3993, Sept. 2018.

[15] F. Wu, L. Zhang and J. Duan, "A New Two-Phase Stationary-Frame-Based Enhanced PLL for Three-Phase Grid Synchronization," *IEEE Trans. Circuits and Syst.*, vol. 62, no. 3, pp. 251-255, March 2015.

[16] T. A. Youssef and O. Mohammed, "Adaptive SRF-PLL with reconfigurable controller for Microgrid in grid-connected and stand-alone modes," *IEEE Power & Energy Society General Meeting*, pp. 1-5, 2013.

[17] R. Diversi, R. Guidorzi and U. Soverini, "Kalman filtering in extended noise environments," *IEEE Trans. Auto. Control*, vol. 50, no. 9, pp. 1396-1402, Sept. 2005.

[18] R. K. Agarwal, I. Hussain, and B. Singh, "LMF-based control algorithm for single stage three-phase grid integrated solar PV system," *IEEE Trans. Sustain. Energy*, vol. 7, no. 4, pp. 1379–1387, Oct. 2016.

[19] P. Chittora, A. Singh and M. Singh, "Simple and efficient control of

DSTATCOM in three-phase four-wire polluted grid system using MCCF-SOGI based controller," *IET Generation, Transmission & Distribution*, vol. 12, no. 5, pp. 1213-1222, 2018.

[20] H. Xiang, B. Chen, M. Yang and C. Li, "Altitude measurement based on characteristics reversal by deep neural network for VHF radar," *IET Radar, Sonar Navig.*, vol. 13, no. 1, pp. 98-103, Jan. 2019.

[21] J. Mazumdar, R. G. Harley and G. K. Venayagamoorthy, "Synchronous Reference Frame Based Active Filter Current Reference Generation Using Neural Networks," *Proc. IEEE IECON 2006*, pp. 4404-4409, 2006.

[22] R. K. Agarwal, I. Hussain and B. Singh, "Application of LMS-Based NN Structure for Power Quality Enhancement in a Distribution Network Under Abnormal Conditions," in *IEEE Trans. Neural Networks and Learning Sys.*, vol. 29, no. 5, pp. 1598-1607, May 2018.

[23] B. Singh and S. R. Arya, "Back-Propagation Control Algorithm for Power Quality Improvement Using DSTATCOM," *IEEE Trans. Indus. Electr.*, vol. 61, no. 3, pp. 1204-1212, March 2014.

[24] A. Yaguchi, T. Suzuki, W. Asano, S. Nitta, Y. Sakata and A. Tanizawa, "Adam Induces Implicit Weight Sparsity in Rectifier Neural Networks," *Proc. IEEE Int. Conf. Machine Learn. Appl. (ICMLA)*, pp. 318-325, 2018.

[25] B. Singh, Chandra, and K. Al-Hadad, '*Power Quality: Problems and Mitigation Techniques*', John Wiley & Sons Ltd., U. K., 2015.

[26] Recommended Practices and Requirements for Harmonic Control on Electric Power System, IEEE Standard 519, IEEE, 2014.

Pavitra Shukl (M'17) was born in New Delhi, India in 1990. She received her B.Tech degree in Electrical Engineering from Bundelkhand Institute of Engineering and Technology, Jhansi, India in 2013 and M.Tech degree (Gold Medalist) in Electrical Power System and Management from Jamia Millia Islamia (A Central University), New Delhi, India in 2016. She is currently working towards her Ph.D. degree in the department of Electrical Engineering, Indian Institute of Technology Delhi, New Delhi, India. Her areas of research interests include solar energy generation system, power electronics, application of adaptive and intelligent control for power quality improvement of the renewable power generation and application of soft computing techniques in power system.

Bhim Singh (SM'99, F'10) was born in Rahamapur, Bijnor (UP), India, in 1956. He has received his B.E. (Electrical) from the University of Roorkee (Now IIT Roorkee), India, in 1977 and his M.Tech. (Power Apparatus & Systems) and Ph.D. from the Indian Institute of Technology Delhi, India, in 1979 and 1983, respectively.

In 1983, he joined the Department of Electrical Engineering, University of Roorkee, as a Lecturer. He became a Reader there in 1988. In December 1990, he joined the Department of Electrical Engineering, IIT Delhi, India, as an Assistant Professor, where became an Associate Professor in 1994 and Professor in 1997. He has been ABB Chair Professor from September 2007 to September 2012. He has also been CEA Chair Professor from October 2012 to September 2017. He has been the Head of the Department of Electrical Engineering at IIT Delhi from July 2014 to August 2016. Since, August 2016, he is the Dean, Academics at IIT Delhi.

Prof. Singh has guided 79 Ph.D. dissertations, and 166 M.E./M.Tech./M.S.(R) theses. He has filed 41 patents. He has executed more than eighty sponsored and consultancy projects. He has co-authored a text book on power quality: Power Quality Problems and Mitigation Techniques published by John Wiley & Sons Ltd. 2015.

His areas of interest include solar PV grid interface systems, microgrids, power quality monitoring and mitigation, solar PV water pumping systems, improved power quality AC-DC converters, power electronics, electrical machines, drives, flexible alternating transmission systems, and high voltage direct current systems.

He has received Khosla Research Prize of University of Roorkee in the year 1991. He is recipient of JC Bose and Bimal K Bose awards of The Institution of Electronics and Telecommunication Engineers (IETE) for his contribution in the field of Power Electronics. He is also a recipient of Maharashtra State National Award of Indian Society for Technical Education (ISTE) in recognition of his outstanding research work in the area of Power Quality. He has received PES Delhi Chapter Outstanding Engineer Award for the year 2006. Professor Singh has received Khosla National Research Award of IIT Roorkee in the year 2013. He is a recipient of Shri Om Prakash Bhasin Award-2014 in the field of Engineering including Energy & Aerospace. Professor Singh has received IEEE PES Nari Hingorani Custom Power Award-2017. He is also a recipient of "Faculty Research Award as a Most Outstanding Researcher" in the field of Engineering-2018 of Careers-360, India. He has received Faculty Lifetime Research Award-2018 for overall research contribution at IIT Delhi.